

Tensor network states in time-bin quantum optics

Michael Lubasch,¹ Antonio A. Valido,² Jelmer J. Renema,¹ W. Steven Kolthammer,²
Dieter Jaksch,^{1,3} Myungshik S. Kim,² Ian Walmsley,¹ and Raúl García-Patrón⁴

¹*Clarendon Laboratory, Department of Physics, University of Oxford, Oxford OX1 3PU, United Kingdom*

²*QOLS, Blackett Laboratory, Imperial College London, London SW7 2AZ, United Kingdom*

³*Center for Quantum Technologies, National University of Singapore, 117543 Singapore*

⁴*Centre for Quantum Information and Communication, Ecole Polytechnique de Bruxelles, CP 165, Université Libre de Bruxelles, 1050 Brussels, Belgium*

(Dated: June 15, 2022)

The current shift in the quantum optics community towards large-size experiments – with many modes and photons – necessitates new classical simulation techniques that go beyond the usual phase space formulation of quantum mechanics. To address this pressing demand we formulate linear quantum optics in the language of tensor network states. As a toy model, we extensively analyze the quantum and classical correlations of time-bin interference in a single fiber loop. We then generalize our results to more complex time-bin quantum setups and identify different classes of architectures for high-complexity and low-overhead boson sampling experiments.

PACS numbers: 02.70.-c, 03.67.-a, 42.50.Ar, 42.81.-i

I. INTRODUCTION

In recent years, interest within the quantum information processing community has shifted from full universal quantum computation to smaller scale tasks which can be run on non-universal computers, which require fewer resources and which might be built with present technology [1]. Linear quantum optics, through the boson sampling proposal [2], is a paradigmatic example of a platform suitable for such non-universal processing tasks: While a linear optical network consisting solely of sources, an interferometer, and a final array of detectors is not able to implement universal quantum computation, it can implement a problem where a quantum machine outperforms a classical one. The initial boson sampling proposal [2] concerns a specific experimental arrangement of a planar linear-optics interferometer capable of implementing a random linear optics interferometer, which raises the question of the computational potential of other linear optical setups.

A promising candidate for the implementation of large-scale photonic quantum interference is time-bin quantum optics [3]. In time-bin quantum optics, the quantum information is encoded in the temporal degrees of freedom, i.e. arrival times, of photons rather than in their spatial degrees of freedom, as is conventionally done. The strong experimental advantage of this approach is that the same sources and detectors can be repeatedly reused in the same experiment, bringing down experimental overheads. Various experimental techniques have been proposed to implement mode mixing between adjacent temporal modes, including orbital angular momentum [4, 5] and dispersion [6], but the most common technique is temporal delays, usually experimentally realized by a network of fiber loops [3] – an example is shown in Fig. 1 (a). Such networks of fiber loops have been used for boson sampling [7, 8] as well as for realization of multidimensional quantum walks [9], large-scale quan-

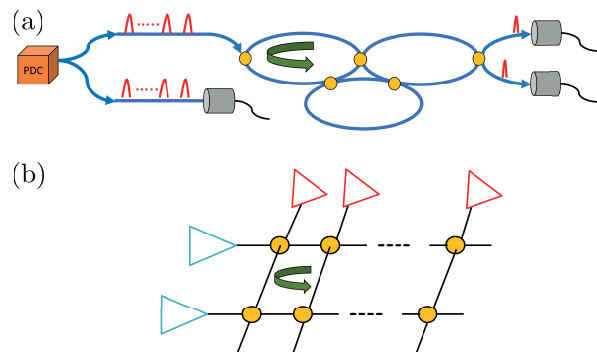


FIG. 1. (a) A quantum optical interferometer is composed of: a heralded photon source, i.e. a parametric-down-conversion source (orange box *PDC*) generating pairs of photons that are heralded by photon-counting detectors on the ancillary mode; a series of interferometric loops (green arrow) interconnected by couplers (yellow circles) mediating the interaction between optical loops; a set of outputs that are photo-counted. (b) Using the techniques described in this article one can build the tensor network state corresponding to an optical interferometer. Every node in the graph is a tensor representing either an input state (red triangle for a time-bin input state and blue triangle for an initial loop state), a coupling or local phase operation (yellow circle), or a measurement outcome. The edges are causal connections between those elements and correspond to tensor contractions.

tum walks [10], and continuous-variable quantum information processing [11].

The complexity¹ of the information processing which such a network can implement depends on the nature of

¹ In this article we use the notion of complexity in a general sense to describe systems or problems that are hard to simulate or solve. We use the notion of computational cost to denote upper bounds on the scaling of the running time and memory require-

the coupling between the adjacent time-bin modes. If we allow the coupling between adjacent modes to change with each time step, then it is known that an arbitrary interferometer can be implemented [7], and hence the hardness of sampling from the output state of such a system follows from Ref. [2]. However, such control might not be always achievable, especially if low-loss operation is desired. Fast modulation requires the use of the electro-optic effect, and it has proven difficult to implement a low-loss modulator based on this effect due to the technical difficulty of realizing low-loss lithium niobate waveguides [12–14]. There is therefore interest in asking what degree of complexity can be achieved by static couplers, i.e. couplers that have a constant value throughout the experiment.

In this work, we analyze the complexity of such static time-bin experiments with the help of tensor network states. Tensor network states – also known as tensor networks – have become a powerful theoretical framework that allows us to efficiently represent non-trivial quantum states, operations and solve optimization problem, such as approximately finding the ground state energy – Refs. [15–18] provide very complete presentations of tensor network states. In the tensor network language, the quantum state or operation is represented by a graph where nodes correspond to tensors and edges determine the rules for the tensor contraction that gives the desired result. The central numerical ingredient in all tensor network computations is the contraction of possibly large products of tensors. The computational cost of these tensor product contractions increases with the number of closed loops contained in the tensor network graph. We show in this work that there exists a connection between loops in a quantum optical interferometer and loops in its corresponding tensor network description. This connection can be used to learn something about the computational complexity of a boson sampling experiment.

Our results consist of three parts. First, we formalize the connection between time-bin interferometers and tensor networks. Building on previous work [19–22] we show that a quantum optical setup can be transformed directly into a tensor network state. Second, we consider the states generated by the simplest possible time-bin system: a single fiber loop. In the tensor network formalism this is represented by a matrix product state. Matrix product states are part of the set of numerically tractable tensor networks which can prove useful for many interesting quantum optical applications such as e.g. metrology or sensing [23]. Finally, we discuss sufficient conditions for the efficient classical simulation of tensor network states and how they can be exploited to design time-bin interferometers as novel candidates for a quantum advantage experiment.

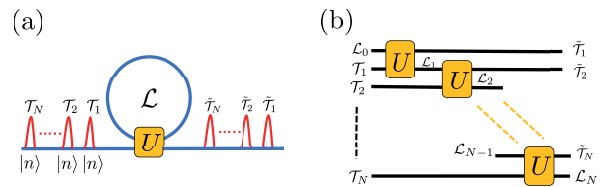


FIG. 2. (a) A single fiber loop with internal degree of freedom \mathcal{L} interacts with N input time-bin modes \mathcal{T}_i through a time-invariant coupler implementing the unitary U given in Eq. (1). This process has N output time-bin modes $\tilde{\mathcal{T}}_i$. (b) A circuit representation unfolding the fiber loop interaction with the N time-bin modes. The circuit is composed of a ladder of identical coupler gates realizing the unitary interaction U between the time-bin mode \mathcal{T}_i and the fiber loop mode \mathcal{L}_i at time i . Note that in the circuit representation the fiber loop system \mathcal{L} moves one step down the ladder after every coupling interaction.

II. SINGLE FIBER LOOP

The central topic of this article is time-bin quantum optical interferometry which has as its most basic element the single fibre loop, shown in Fig. 2 along with its representation as a planar quantum circuit. This system is composed of a single time delay \mathcal{L} – which is the fiber loop – and a pulse train on N time-bin modes \mathcal{T}_i that are equally spaced and sequentially interact with the fiber loop \mathcal{L} through a coupler at time-steps Δt . Such a system is experimentally realized by setting the length of the loop equal to the distance light travels between two input time-bins, in order to achieve temporal overlap between photons entering the loop at time step i and photons arriving at time step $i+1$. The interference between modes i and $i+1$ is mediated by a time-independent coupler that implements an interaction $U : \mathcal{H}_{\mathcal{T}_i} \otimes \mathcal{H}_{\mathcal{L}} \rightarrow \mathcal{H}_{\tilde{\mathcal{T}}_i} \otimes \mathcal{H}_{\tilde{\mathcal{L}}}$, where we have used the tilde in $\tilde{\mathcal{T}}/\tilde{\mathcal{L}}$ to denote the output nature of that mode. The coupling interaction is the well-known passive bosonic hopping interaction [24, 25] equivalent to a beam splitter:

$$\hat{U}(\theta, \phi) := e^{\theta(\hat{a}^\dagger \hat{b} e^{i\phi} - \hat{a} \hat{b}^\dagger e^{-i\phi})} \quad , \quad (1)$$

where \hat{a} and \hat{b} are the loop and time-bin annihilation operators, ϕ represents a phase between the output modes, and θ parametrizes the intensity transmission and reflection probabilities $\cos^2(\theta)$ and $\sin^2(\theta)$, respectively. This system will be explained and analyzed in detail in Sec. IV, with the aim to gently introduce tensor network states to the quantum optics community. There we will also present some subtleties that appear in tensor network simulations of quantum optics.

III. TENSOR NETWORK STATES

Tensor network states – also called tensor networks – have proven to be a very successful approach for the

ments of an algorithm. And we use the notion of computational complexity or hardness for results that were obtained via rigorous proofs using complexity theory.

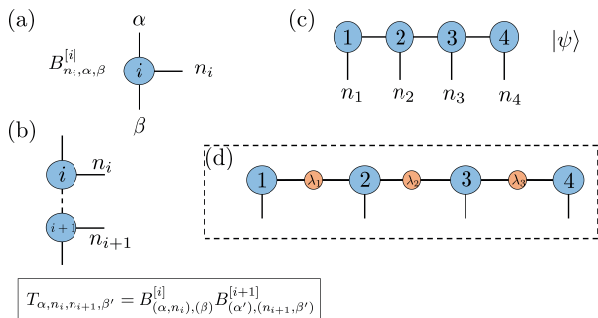


FIG. 3. (a) An example of a tensor $B_{n_i, \alpha, \beta}^{[i]}$ of rank three: represented by a vertex i with three edges for the three indices n_i , α , and β . For the quantum optical problems discussed in this article, the index n_i represents a physical quantity – namely the number of photons in time-bin mode \mathcal{T}_i – and the indices α and β represent virtual quantities – encoding the correlations between adjacent time-bin modes. (b) The tensor contraction of $B^{[i]}$ and $B^{[i+1]}$ along their shared index (dashed line) is an operation equivalent to matrix multiplication along the shared index, as explained in the main text. (c) Graphical representation of a quantum state $|\psi\rangle$ corresponding to a matrix product state of four tensors, as defined in Eq. (2). (d) All matrix product states can be transformed into a canonical form where a diagonal matrix λ of Schmidt coefficients is assigned to every edge of the matrix product state, see Eq. (3) and corresponding discussion.

study of quantum many-body states and operations [15–18]. They allow us to carry out non-trivial calculations for large many-body systems: e.g. they allow us to compute expectation values of operators, overlaps between quantum states, approximate time evolution of quantum states, and much more. And one of the most successful numerical algorithms for the ground state computation of one-dimensional quantum many-body systems, the density matrix renormalization group [26, 27], can be reformulated as a variational algorithm over tensor network states [28–30].

The central ingredient of all tensor network calculations is the tensor contraction, i.e. a generalization of vector and matrix multiplication to tensors of arbitrary rank. An example is shown in Fig. 3. The contraction of the two tensors $B^{[i]}$ and $B^{[i+1]}$ along their shared index, as shown in Fig. 3 (b), can be implemented in two steps: firstly, we transform the two tensors $B^{[i]}$ and $B^{[i+1]}$ into two matrices by merging all non-contracted indices into single indices, i.e., α and n_i in $B_{(\alpha, n_i), (\beta)}^{[i]}$, and β' and n_{i+1} in $B_{(\alpha'), (n_{i+1}, \beta')}^{[i+1]}$, into a single one, which transforms the two tensor into two matrices; secondly, we multiply both matrices $B_{(\alpha, n_i), (\beta)}^{[i]}$ and $B_{(\alpha'), (n_{i+1}, \beta')}^{[i+1]}$ over their shared index, i.e. β for $B_{[i]}$ and α' for $B_{[i+1]}$. The result of this tensor contraction is a new tensor $T_{\alpha, n_i, n_{i+1}, \beta'}$ of rank four.

One of the most widely used tensor network states is shown in Fig. 3 (c): a matrix product state [28, 31–33].

This is a one-dimensional tensor network that can e.g. represent a quantum state $|\psi\rangle$. Let us consider a quantum state composed of N quantum systems each living in a d -dimensional Hilbert space and let us denote the computational basis states of the individual quantum systems i by $|n_i\rangle$ where $n_i \in \{0, 1, \dots, d-1\}$. Then a matrix product state takes on the form:

$$|\psi\rangle = \sum_{n_1, n_2, \dots, n_N} \left(B_{n_1}^{[1]} B_{n_2}^{[2]} \dots B_{n_N}^{[N]} \right) |n_1, n_2, \dots, n_N\rangle \quad (2)$$

where the sum $\sum_{n_1, n_2, \dots, n_N} := \sum_{n_1=0}^{d-1} \sum_{n_2=0}^{d-1} \dots \sum_{n_N=0}^{d-1}$ runs over all basis states $|n_1, n_2, \dots, n_N\rangle$. Here, $B_{n_1}^{[1]}$ is a transposed vector of dimension χ_1 , $B_{n_N}^{[N]}$ is a vector of dimension χ_N , and $B_{n_i}^{[i]}$ for $1 < i < N$ is a matrix of dimension $\chi_{i-1} \times \chi_i$. Thus in a matrix product state the wave function coefficient for a specific basis state $|n_1, n_2, \dots, n_N\rangle$ is given by a vector-matrix-matrix-...-matrix-vector product $B_{n_1}^{[1]} B_{n_2}^{[2]} B_{n_3}^{[3]} \dots B_{n_{N-1}}^{[N-1]} B_{n_N}^{[N]}$.

The dimensions χ_i are important parameters in matrix product state computations as they determine the computational cost of storing and processing matrix product states. We define $\chi := \max_i(\chi_i)$ and call this the bond dimension. Then the total number of parameters and thus the computational cost of storage for such a matrix product state scales as $\mathcal{O}(Nd\chi^2)$. The computational cost of processing such a matrix product state depends on the details of the algorithm. However, most matrix product state algorithms – for matrix product states with open boundary conditions as considered here – have a computational cost scaling like $\mathcal{O}(Nd\chi^3)$ [15, 18].

The bond dimension also determines the amount of entanglement that a matrix product state can contain. Every matrix product state can be transformed into a canonical form [32, 33]

$$\sum_{n_1, n_2, \dots, n_N} \left(\Gamma_{n_1}^{[1]} \lambda^{[1]} \Gamma_{n_2}^{[2]} \lambda^{[2]} \dots \Gamma_{n_N}^{[N]} \right) |n_1, n_2, \dots, n_N\rangle \quad (3)$$

in which the $\lambda^{[i]}$ are diagonal matrices containing the Schmidt coefficients for the matrix product state bipartition between sites $1, 2, \dots, i$ and $i+1, i+2, \dots, N$ – a very comprehensive presentation of Schmidt decomposition and coefficients is given in Ref. [34]. A graphical representation of a matrix product state in canonical form is sketched in Fig. 3 (d). The canonical form allows us to compute the entanglement entropy [35, 36] for every bipartition of the matrix product state as

$$E(i) := - \sum_{k=0}^{\chi_i-1} (\lambda_k^{[i]})^2 \log((\lambda_k^{[i]})^2) \quad . \quad (4)$$

The entanglement entropy plays an important role in tensor network simulations of many-body systems. Eq. (4) tells us that a matrix product state of bond dimension χ can never have values of E larger than $\log(\chi)$. Therefore, when a many-body system contains large amounts of entanglement, then the matrix product state simulation requires large values of χ and thus

has a high computational cost. Thus entanglement can be used as an indicator for the hardness of the classical simulation based on matrix product states [37].

Besides matrix product states, there exist many other interesting types of tensor networks, and some of the most widely used tensor network types are explained in Refs. [15, 16, 18]. Of particular importance for this article are projected entangled pair states [38, 39] which represent a very natural generalization of matrix product states to higher dimensions. Projected entangled pair states can contain much more entanglement than matrix product states and their exact tensor network contraction is known to be computationally hard [40]. However, efficient approximate tensor network contractions of projected entangled pair states are feasible, see e.g. Refs. [15, 18, 38, 39, 41, 42]. We shall learn later in Sec. V A how projected entangled pair states can be generated with fiber loops.

Tensor network techniques can be applied to quantum optics in different ways [19–22]. In this article we map time-bin quantum optical setups to their corresponding tensor network state by identifying the time-bin modes as the individual quantum systems in the tensor network description. Then each time-bin mode \mathcal{T}_i is described by a d -dimensional Hilbert space and bosonic mode occupation numbers $n_i \in \{0, 1, \dots, d-1\}$. Therefore our tensor network description implies a maximally possible bosonic mode occupation number $n_{\max} = d-1$ for each time-bin mode. At first glance, this seems to be a strong restriction for a general quantum optical setup in which e.g. photon bunching might occur and thus a large bosonic mode occupation number might appear in a single time-bin mode. However, we will see in the next Sec. IV that this is not a problem for tensor network algorithms. The parameters d and χ are always chosen large enough to capture the true physics. This is achieved by successively increasing d and χ until all results do not change anymore and have thus become independent of d and χ .

IV. EFFICIENT CLASSICAL SIMULATION OF FIBER LOOPS

One of the most successful methods for the simulation of quantum states of light is based on the phase-space representation of quantum states [43]. This method can efficiently simulate the evolution of multi-mode Gaussian states under Gaussian operations, both unitary and noisy

channels, and the quadratures of the fields [44, 45]. It can also be adapted to simulate some classes of non-Gaussian states, such as e.g. non-Gaussian probabilistic mixtures of Gaussian states [46] or extremely noisy regimes [47]. However, the calculations quickly become cumbersome if one wants to model superpositions of many photon numbers or multi-mode entangled non-Gaussian states.

To address the need for efficient simulations of multi-mode and multi-photon experiments – for which the previous simulation techniques are not powerful enough – we suggest the use of tensor networks, which might become as powerful for these quantum optics simulations as they are already in many-body physics. In this section we illustrate how tensor networks can be used in quantum optics to analyze the interaction of N time-bin modes over a single fiber loop. Such a system takes on the form of a matrix product state. Using this matrix product state description, we show how entanglement and correlations are computed and explain how boson sampling can be done efficiently on a classical computer.

A. Matrix product states from a single fiber loop

It is easy to see that the single fiber loop architecture corresponds to a sequential interaction between an ancillary system, represented here by the fiber loop \mathcal{L} , and a train of input systems, represented here by the time-bin modes \mathcal{T}_i . This sequential process can be naturally modeled by a matrix product state [48, 49], see also Fig. 4.

For a train of N input time-bin modes \mathcal{T}_i in the multi-mode Fock state $|n_1\rangle \otimes |n_2\rangle \otimes \dots \otimes |n_N\rangle$ the final state reads

$$|\psi\rangle = V^{[N]}V^{[N-1]} \dots V^{[2]}V^{[1]}|\varphi\rangle_{\mathcal{L}} \quad . \quad (5)$$

Here $|\varphi\rangle_{\mathcal{L}}$ denotes the initial state of the loop which we always set to be the vacuum state $|0\rangle$ and $V^{[i]}$ denotes the isometry obtained from U of Eq. (1) after action of the time-bin input state $|n_i\rangle$:

$$\begin{aligned} V^{[i]} &:= \hat{U}|n_i\rangle_{\mathcal{T}} \\ &= \sum_{o,p,q} U_{n_i,o}^{p,q} |o\rangle_{\tilde{\mathcal{L}}} |p\rangle_{\tilde{\mathcal{T}}} \langle q|_{\mathcal{L}} \quad , \end{aligned} \quad (6)$$

where $\mathcal{L}/\tilde{\mathcal{L}}$ denotes the loop input/output and $\mathcal{T}/\tilde{\mathcal{T}}$ denotes the time-bin input/output mode of U . If we write all output modes explicitly then Eq. (5) turns into

$$|\psi\rangle = \sum_{n_1, n_2, \dots, n_N, n_{\tilde{\mathcal{L}}}} V_{n_{\tilde{\mathcal{L}}}, n_N}^{[N]} V_{n_{N-1}}^{[N-1]} \dots V_{n_2}^{[2]} V_{n_1}^{[1]} |\varphi\rangle_{\mathcal{L}} |n_{\tilde{\mathcal{L}}}, n_N, \dots, n_2, n_1\rangle \quad (8)$$

where $|\varphi\rangle_{\mathcal{L}} = |0\rangle$ acts only on the loop input mode of $V^{[1]}$ and $|n_{\tilde{\mathcal{L}}}\rangle$ represents the loop output mode of $V^{[N]}$.

This fiber loop matrix product state is shown in Fig. 4 (b).

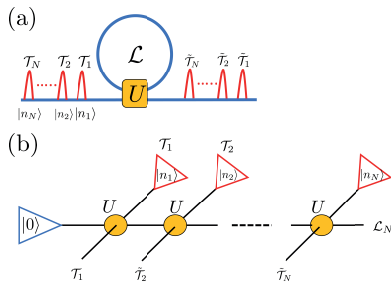


FIG. 4. (a) A single fiber loop with internal degree of freedom \mathcal{L} interacts with N input time-bin modes \mathcal{T}_i through a time-invariant coupler implementing the unitary U of Eq. (1). The result of this process are N output time-bin modes $\tilde{\mathcal{T}}_i$. (b) Tensor network representation of the output state of the N time-bin modes and the loop at step N . Each yellow circle corresponds to a tensor with two input and two output indices where each index represents either an input or output degree of freedom of the coupling interaction U . The blue and red triangles correspond to vectors, i.e. tensors of rank one, that represent the input states of the loop and time-bins, respectively.

Our numerical construction of this fiber loop matrix product state starts from Eq. (1). We assume a d -dimensional Hilbert space for each mode of U . Then the annihilation and creation operators \hat{a} , \hat{b} , \hat{a}^\dagger , and \hat{b}^\dagger can each be written as a $d \times d$ -dimensional matrix. After numerically computing the matrix exponential for U , we reshape U into a tensor of rank four, i.e. having four indices. By contracting the correct input indices with the input states described in the previous paragraph we obtain the tensors $V^{[i]}$ of our fiber loop matrix product state. Note that in this fiber loop matrix product state $\chi = d$.

B. Entanglement and area law

The amount of entanglement contained in a randomly selected quantum many-body state typically grows with the number of its constituents N , see e.g. Ref. [15] and references therein. E.g. the entanglement entropy E of such a state – for a bipartition of the complete state into two equally large parts – typically grows linearly with N . However, not all quantum many-body states contain these large amounts of entanglement. E.g. ground states of local, gapped Hamiltonians in one spatial dimension are characterized by an amount of E that saturates with increasing N to a final constant value that is independent of N [50]. In this case the entanglement entropy fulfills $E \leq C$ for a constant that is independent of N and so entanglement entropy satisfies an area law, i.e. it grows with N at most like the area between the two subsystems of the bipartition (note that in one spatial dimension the area between the two subsystems of the bipartition is a constant independent of N) – Ref. [51] provides a very comprehensive presentation of the area

law from the perspective of quantum many-body physics. As we have seen in Sec. III, matrix product states of bond dimension χ can only have values of entanglement entropy $E \leq \log(\chi)$ that fulfill the area law whenever χ is a constant independent of the size of the system. This is enough for ground states of local, gapped Hamiltonians in one spatial dimension, and matrix product states indeed allow us to efficiently and accurately approximate such ground states [50, 52, 53].

However, for our single fiber loop it is a priori not clear that entanglement entropy satisfies an area law and matrix product states provide an accurate description. The true Hilbert space dimension of the loop mode is infinite, and so the loop could accommodate more and more photons when N grows, as more and more photons could enter the loop. This could potentially lead to a violation of the entanglement area law and in our matrix product state description would require larger values of d for increasing N . The following theorem and corollary prove that this is not the case: matrix product states provide an efficient and accurate description for a single fiber loop.

Theorem 1. For a train of N input time-bin modes \mathcal{T}_1 to \mathcal{T}_N in the multi-mode Fock state $|n_1\rangle \otimes |n_2\rangle \otimes \dots \otimes |n_N\rangle$ acting on a single fiber loop, the entanglement entropy $E(i)$ of Eq. (4) for a bipartition between output time-bin modes $\tilde{\mathcal{T}}_1$ to $\tilde{\mathcal{T}}_i$ and $\tilde{\mathcal{T}}_{i+1}$ to $\tilde{\mathcal{T}}_N$ for any time-bin i is upper-bounded by $g(n(i))$ where $n(i)$ denotes the average photon number inside the fiber loop in time-bin i and

$$g(n) := (1+n) \log_2(1+n) - n \log_2(n) \quad . \quad (9)$$

Proof. For every time-bin i , the state of the output fiber loop mode and the output time-bin modes $\tilde{\mathcal{T}}_1$ to $\tilde{\mathcal{T}}_i$ can be written as a Schmidt decomposition. The squared Schmidt coefficients are the eigenvalues of the reduced density matrix characterizing the fiber loop mode in time-bin i . They allow us to compute the entanglement entropy $E(i)$ for the bipartition between the output fiber loop mode and the output time-bin modes $\tilde{\mathcal{T}}_1$ to $\tilde{\mathcal{T}}_i$ using Eq. (4). For any future time-bin $i+j$ where $j > 0$, the entanglement entropy for the bipartition between the output time-bin modes $\tilde{\mathcal{T}}_1$ to $\tilde{\mathcal{T}}_i$ and the output fiber loop mode together with the output time-bin modes $\tilde{\mathcal{T}}_{i+1}$ to $\tilde{\mathcal{T}}_{i+j}$ is determined by the previous eigenvalues of the reduced density matrix of the fiber loop mode in time-bin i . This is true because the input time-bin modes are a product state and the coupler is unitary. So the entropy of the output fiber loop mode in time-bin i is equivalent to the entropy of the output fiber loop mode together with output time-bin modes $\tilde{\mathcal{T}}_{i+1}$ to $\tilde{\mathcal{T}}_{i+j}$ in time-bin $i+j$. Finally, we exploit the fact that among all states of the same average photon number the thermal state maximizes the entropy [54] (see also Ref. [55]) given by Eq. (9). ■

Corollary 1. The entanglement entropy E for any bipartition of the output state of a single fiber loop for an input multi-mode Fock state $|n_1\rangle \otimes |n_2\rangle \otimes \dots \otimes |n_N\rangle$ satisfies an area law: $E \leq g(\max_i(n_i))$. For an input state

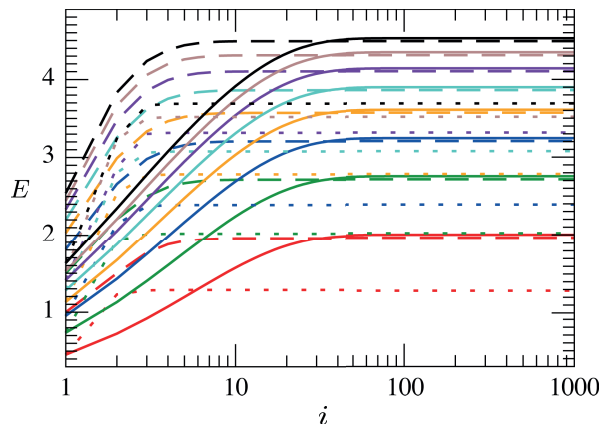


FIG. 5. Entanglement entropy E as a function of time i for $\theta = 0.4\pi$ (dotted), 0.25π (dashed), and 0.1π (solid), and $n = 1$ (red), 2 (green), 3 (blue), 4 (orange), 5 (turquoise), 6 (violet), 7 (brown), and 8 (black). Our results are converged with increasing length N and tensor dimensions d and χ of the matrix product state: we used $N = 1100$ and $d = 81 = \chi$. We computed the entanglement entropy via the canonical form of Eq. (3) and the formula of Eq. (4).

composed of the same number of photons n in each input time-bin mode, this implies: $E \leq g(n)$.

Proof. Given $n(i)$ the mean photon number in the loop in time-bin i and n_{i+1} the input photon number in time-bin $i + 1$, the average photon number in the fiber loop in time-bin $i + 1$ is given by $n(i + 1) = \cos^2(\theta)n(i) + \sin^2(\theta)n_{i+1}$. This implies the bound $n(i + 1) \leq \max(n(i), n_{i+1})$. Thus, for the input multi-mode Fock state $|n_1\rangle \otimes |n_2\rangle \otimes \dots \otimes |n_N\rangle$ we obtain $n(i) \leq \max_{j \leq i}(n_j)$. This together with the previous theorem proves the area law for entanglement entropy: $E \leq g(\max_i(n_i))$. ■

Using the matrix product state representation of the single fiber loop setup, we have performed several numerical calculations that are presented in the following. We programmed all required tensor network routines in the Tensor Network Theory Library [56, 57]. In all our numerical computations we assumed that every input time-bin mode \mathcal{T}_i has the same photon number n , i.e. in the input multi-mode Fock state $|n_1\rangle \otimes |n_2\rangle \otimes \dots \otimes |n_N\rangle$ we set $n_i = n$ for all i . Furthermore, we always chose $\chi = d$, and all numerical results were converged with increasing values of d .

Figure 5 shows the entanglement entropy $E(i)$ of the fiber loop mode in time-bin i for different values of n and θ . We observe that entanglement grows with time until it saturates at a final value that depends on n and θ . For a fixed value of θ , entanglement grows with increasing n . For a fixed value of n , smaller θ lead to larger final amounts of entanglement but require longer saturation times. Because $E(i)$ saturates at a constant value for large values of i , i.e. after long enough time, this suggests that entanglement entropy has an upper bound independent of N and thus satisfies an area law. This ef-

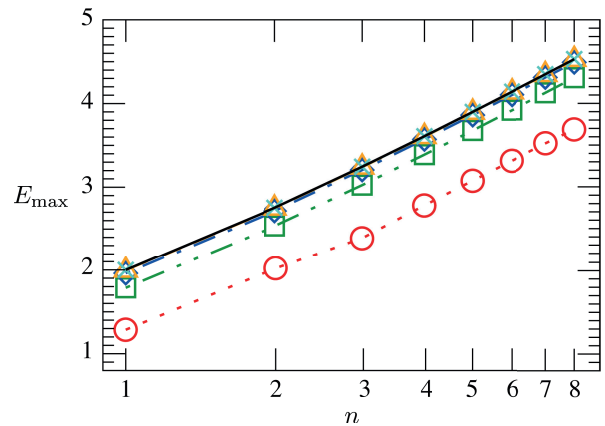


FIG. 6. Maximum entanglement entropy E_{\max} as a function of n for $\theta = 0.4\pi$ (circles, dotted), $\pi/3$ (squares, dash-dotted), 0.25π (diamonds, dash-dotted), $\pi/6$ (triangles, dashed), 0.1π (crosses, solid), and the analytical upper bound $(1 + n) \log_2(1 + n) - n \log_2(n)$ of Eq. (9) (solid). Our results are converged with the same parameters as in Fig. 5 and $E_{\max} := E(i = 1000)$.

fect has an intuitive explanation: The entropy saturates when the loop reaches equilibrium, i.e., when the rate of photons going into the system is equal to the rate with which photons leak out to the detection mode.

Figure 6 confirms the validity of our result on the area law upper bound for entanglement entropy. We observe that the maximum entanglement entropy gets arbitrarily close to the analytical upper bound of Eq. (9) with decreasing value of θ . For each value of θ and the range of n considered here, the dependency of E_{\max} on n is qualitatively well described by $(1 + n) \log_2(1 + n) - n \log_2(n)$.

Figure 7 shows the evolution of entanglement entropy over the full range of possible values for θ . We conclude that for every value of n , entanglement increases quickly with the transmission probability $\cos^2(\theta)$ and is already very close to the maximum possible E when $\cos^2(\theta) > 0.4$. The threshold time $i_{0.95E}$, which is defined in the caption, seems to grow faster than exponentially with $\cos^2(\theta)$. However, between $\cos^2(\theta) = 0.4$ and $\cos^2(\theta) = 0.7$ it takes on relatively small values $i_{0.95E} < 10$. We observe that there exists an interesting trade-off – depending on θ – between the speed of convergence to the entanglement saturation value and how close this value is to the analytical upper bound of Eq. (9). On the one hand, a lower transmission probability leads to faster convergence to the entanglement saturation value – as more photons are injected into the fiber loop in each time-bin – but this saturation value is further away from the analytical upper bound. On the other hand, a higher transmission probability leads to an entanglement saturation value that is the closer to the analytical upper bound but entanglement converges slower to this saturation value.

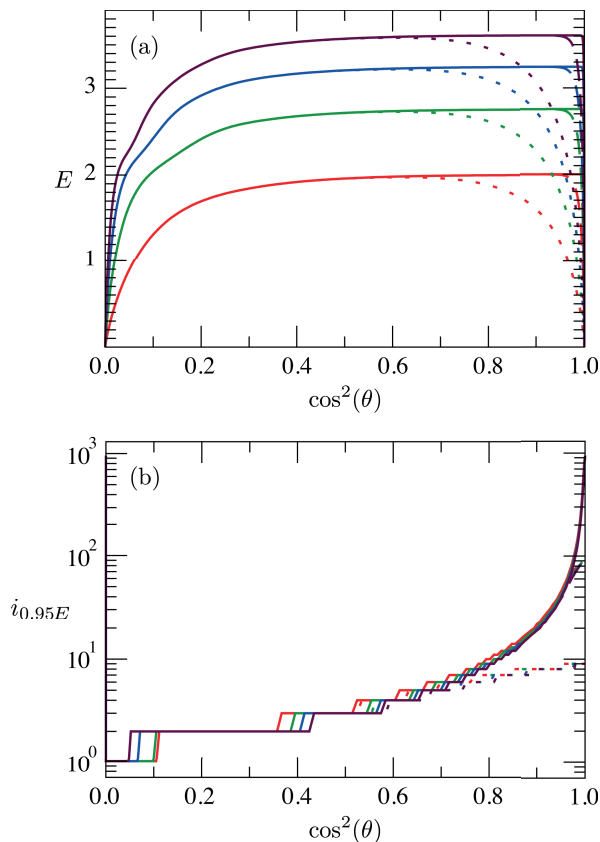


FIG. 7. Entanglement entropy E (a) and threshold time-bin $i_{0.95E}$ (b) as a function of $\cos^2(\theta)$ for $i = 10$ (dotted), 100 (dashed), 1000 (solid), and $n = 1$ (red), 2 (green), 3 (blue), and 4 (purple). The threshold time-bin is defined via $E(i_{0.95E}) > 0.95E(i)$ and $E(i_{0.95E} - 1) < 0.95E(i)$: this quantifies the saturation time. Our results are converged with N , d , and χ : here we used $N = 1100$ and $d = 41 = \chi$.

C. Schmidt coefficients

The remarkable fact that the entanglement saturation value converges to the analytical upper bound of Eq. (9) with decreasing value of θ suggests that the eigenvalues of the reduced density matrix of the fiber loop mode are close to those of the thermal state that provides the exact values for our analytical upper bound. This is compared in Fig. 8 where we plot the Schmidt coefficients for different input photon numbers n and values of θ for a time-bin i after entanglement saturation. Using the Schmidt coefficients λ_k we can easily compute the eigenvalues of the reduced density matrix of the fiber loop mode as λ_k^2 . We conclude that for fixed n the Schmidt values get closer to the thermal state distribution $\sqrt{n^k/(n+1)^{k+1}}$ when the value of θ decreases. All Schmidt coefficients decrease exponentially but with a relatively small coefficient in the exponent. Therefore relatively large values of d and χ are needed for accurate matrix product state representations of these bosonic systems: for all problems considered in this article we observed convergence when

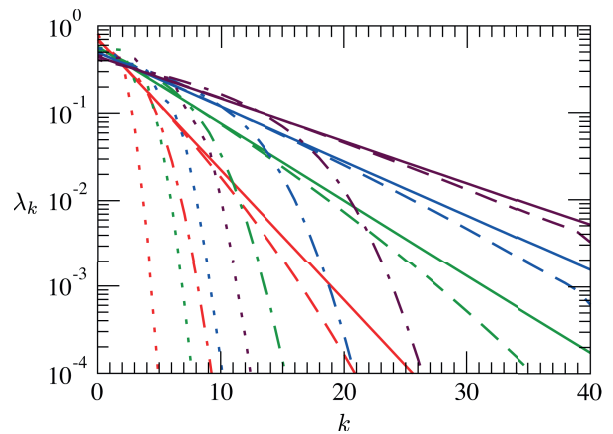


FIG. 8. Schmidt coefficients λ_k for $\theta = 0.4\pi$ (dotted), 0.25π (dash-dotted), 0.1π (dashed), and analytical thermal state distribution $\sqrt{n^k/(n+1)^{k+1}}$ (solid), and $n = 1$ (red), 2 (green), 3 (blue), and 4 (purple). Our results are converged with N , d , χ , and i : we used $N = 1100$, $d = 41 = \chi$, and $i = 1000$.

$$d = \chi = 10n + 1.$$

D. Correlations

In this article we are interested in two-point correlation functions of the form $\langle \hat{n}_i \hat{n}_{i+x} \rangle$, where \hat{n}_i and \hat{n}_{i+x} act on the output time-bin modes \tilde{T}_i and \tilde{T}_{i+x} , respectively. Such expectation values can be computed exactly and efficiently with matrix product states, see e.g. Refs. [15, 18]. The required tensor contractions have a computational cost that scales like $\mathcal{O}(d\chi^3N)$. Figure 9 shows correlation functions computed after convergence with all matrix product state parameters.

In Fig. 9 (a), we observe that the correlation function $C(x) := |\langle \hat{n}_i \hat{n}_{i+x} \rangle - \langle \hat{n}_i \rangle \langle \hat{n}_{i+x} \rangle|$ decreases exponentially with x , as expected from the matrix product state representation, see e.g. Refs. [15, 18]. We read off that the correlation length ζ , which is defined via $C(x) = C_0 \exp(-x/\zeta)$, depends only on θ and not on the input photon number per mode n . n determines the prefactor C_0 . For all our numerical results we have checked explicitly that $C(x)$ can be expressed in terms of the transmission probability $\cos^2(\theta)$ as $C(x) = \tilde{C}_0 (\cos^2(\theta))^x$. Hence for all our numerical results we obtain $\zeta^{-1} = -\ln(\cos^2(\theta))$. We also computed $C(x)$ using the expression from Ref. [58] and found that both for distinguishable photons (i.e. classical photons) and for indistinguishable photons, $C(x)$ exhibits exponential decay, and that the decay constant is identical for the two cases. This shows that the dominant contribution to the exponential decrease of correlations is a classical effect, namely light leaking out of the loop mode over time.

Figure 9 (b) shows the $g^{(2)}$ function $g^{(2)}(x) := \langle \hat{n}_i \hat{n}_{i+x} \rangle / \langle \hat{n}_i \rangle^2$, a well studied quantity in quantum optics

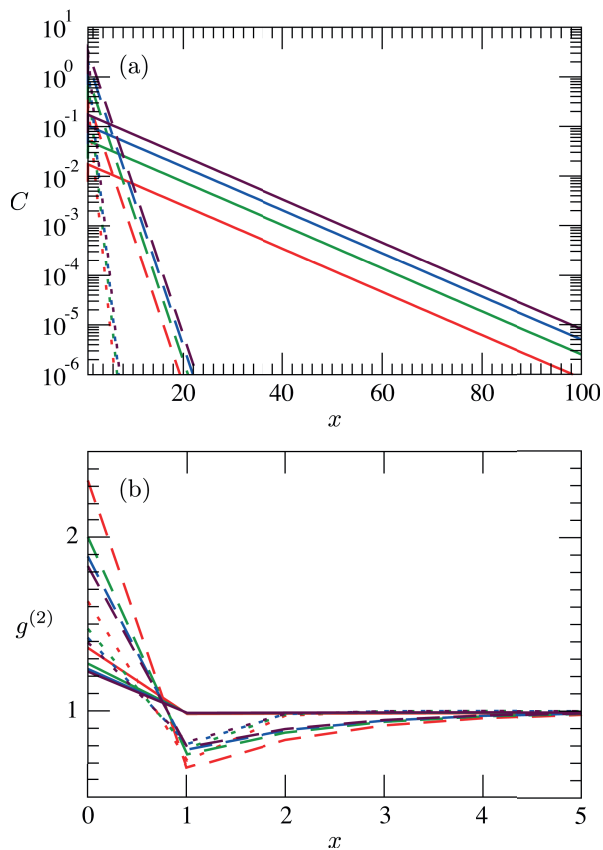


FIG. 9. Correlation functions $C(x) := |\langle \hat{n}_i \hat{n}_{i+x} \rangle - \langle \hat{n}_i \rangle \langle \hat{n}_{i+x} \rangle|$ (a) and $g^{(2)}(x) := \langle \hat{n}_i \hat{n}_{i+x} \rangle / \langle \hat{n}_i \rangle \langle \hat{n}_{i+x} \rangle$ (b) for $\theta = 0.4\pi$ (dotted), 0.25π (dashed), 0.1π (solid), and $n = 1$ (red), 2 (green), 3 (blue), and 4 (purple). Our results are converged with N , d , χ , and i : we used $N = 1100$, $d = 41 = \chi$, and $i = 900$.

that is often used to characterize the non-classicality of light. In all considered cases, we observe $g^{(2)}(x=0) > 1$ and $g^{(2)}(x=0) > g^{(2)}(x > 0)$ and thus bunched light, but a nonclassical $g^{(2)} < 1$ component between adjacent modes.

This picture, obtained using tensor networks, is consistent with that which could have been obtained using the common theoretical framework of quantum optics. Both show that there are quantum effects between closely spaced time-bins, as given by our computed entanglement entropy and $g^{(2)}$ function, but that there is no significant buildup of entanglement (non-classicality) over time, as shown by the saturation of the entanglement entropy. This shows that tensor network states can equivalently reproduce the common theoretical framework of quantum optics and at the same time they can provide novel predictions and accurate descriptions for large quantum states of light.

E. Sampling

Simulating the photon counting statistics of a multi-mode quantum state of light is not an easy task. The objective is to generate samples from the probability distribution $p(n_1, n_2, \dots, n_N)$ where the number of samples is d^N and thus grows exponentially with the number of modes N . This clearly is a daunting task that is, in full generality, classically intractable as shown by the original boson sampling proposal [2]. However, using matrix product states one can overcome this limitation by following a sequential procedure that samples one random outcome per mode at a time and exploits the decomposition of a joint probability distribution as

$$p(n_1, \dots, n_N) = p(n_N | n_{N-1}, \dots, n_1) \dots p(n_2 | n_1) p(n_1). \quad (10)$$

The first step of the algorithm calculates for every value of n_1 – of which there exist $d = n_{\max} + 1$ values – the probability of its outcome $p(n_1) := \langle \psi | (|n_1\rangle\langle n_1| \otimes \mathcal{I}_{2,\dots,N}) | \psi \rangle$, where $|n_1\rangle\langle n_1|$ is the projector onto the photon number state n_1 of mode 1 and $\mathcal{I}_{2,\dots,N}$ is the identity operator on modes 2 to N . In order to compute $p(n_1)$, we contract a tensor network that consists of the matrix product state representing the state as ket $|\psi\rangle$ with the bra $\langle \psi|$ interleaved with a tensor for the projector $|n_1\rangle\langle n_1|$. After we have calculated all d elements of $p(n_1)$, we randomly select one \tilde{n}_1 . Then we update our state by generating $|\psi_{\tilde{n}_1}\rangle := \langle \tilde{n}_1 | \psi \rangle$ where the bra $\langle \tilde{n}_1 |$ acts only on mode 1. The result of this contraction is a new, unnormalized matrix product state $|\psi_{\tilde{n}_1}\rangle$ of size $N - 1$. Note that this new matrix product state satisfies the condition $\langle \psi_{\tilde{n}_1} | \psi_{\tilde{n}_1} \rangle = p(\tilde{n}_1)$.

The second step now uses the state $|\psi_{\tilde{n}_1}\rangle$. Firstly, we calculate the d outcome probabilities $p(n_2, \tilde{n}_1) := \langle \psi_{\tilde{n}_1} | (|n_2\rangle\langle n_2| \otimes \mathcal{I}_{3,\dots,N}) | \psi_{\tilde{n}_1} \rangle$ and randomly select a \tilde{n}_2 from the probability distribution $p(n_2 | \tilde{n}_1) := p(n_2, \tilde{n}_1) / p(\tilde{n}_1)$. Secondly, we generate a new, unnormalized matrix product state $|\psi_{\tilde{n}_1, \tilde{n}_2}\rangle := \langle \tilde{n}_2 | \psi_{\tilde{n}_1} \rangle$ of size $N - 2$. Continuing this procedure for the remaining $N - 3$ output modes, we end up with one sample $(\tilde{n}_1, \tilde{n}_2, \dots, \tilde{n}_N)$ drawn according to the probability distribution $p(n_1, n_2, \dots, n_N)$. Obviously we can generate as many samples as required by running this algorithm several times. All tensor networks encountered in this algorithm can be contracted exactly and efficiently, and the overall computational cost scales as $\mathcal{O}(Md^2\chi^3N^2)$ where M denotes the number of samples.

An alternative simulation strategy, inspired by traditional quantum optics tools, would consider the situation where each output time-bin mode leaving the fiber loop is immediately measured by a photon-number resolving detector. In this case, since photon number is conserved in the interactions in the loop, each measurement of an output mode projects the fiber loop into a Fock state. The physical picture of the system is therefore one of a classical (i.e. non-interfering) random walk over the space of Fock states of the loop, where the transition probability from one Fock state to another is given by the probabil-

ity to observe the generalized Hong Ou Mandel-effect between the Fock state in the loop mode and the incoming photon. It is easy to see that this leads to an algorithm that samples efficiently from the probability distribution $p(n_1, n_2, \dots, n_N)$.

V. ROUTE TO COMPLEXITY

The computational cost of contracting a tensor network depends on the number of closed loops in the graph of that tensor network, see e.g. Refs. [15, 16, 18]. Here the notion of a loop is synonymous to the notion of a simple cycle in graph theory [59].² So if we want to increase the computational complexity of a quantum optical architecture, we need to generate a tensor network state with increasing number of loops. As we will explain in detail below, this can be achieved by increasing the number of interferometric loops, where these loops might have a physical existence in the experimental implementation or result from the interference between different time-bin modes.

A. Tensor network states with multiple loops

We have seen in Sec. IV that a single fiber loop can be represented by a matrix product state, which is a tensor network without cycles, see Fig. 4 (b). In the following we discuss several approaches to increase the computational complexity of the generated tensor network state by adding more interferometric loops to the circuit.

1. Increasing the ancillary system dimension

One example of more complex tensor network states is given by matrix product-like states that have a bond dimension that does not satisfy an area law. As the bond dimension in a matrix product state is related to the dimension of the ancillary system in its sequential generation – see discussion in Sec. IV A – we can increase the computational complexity by enlarging the degrees of freedom of the ancillary system. This can be achieved, e.g., by increasing the number of interconnected fiber loops that interact with the incoming time-bin photons.

Figure 10 shows an example of an ancillary structure composed of two fiber loops. A detailed analysis of the interaction between the input time-bin modes \mathcal{T}_i with both loop modes \mathcal{L}_1 and \mathcal{L}_2 , as sketched in Fig. 10 (a), leads to the circuit diagram shown in Fig. 10 (b). The

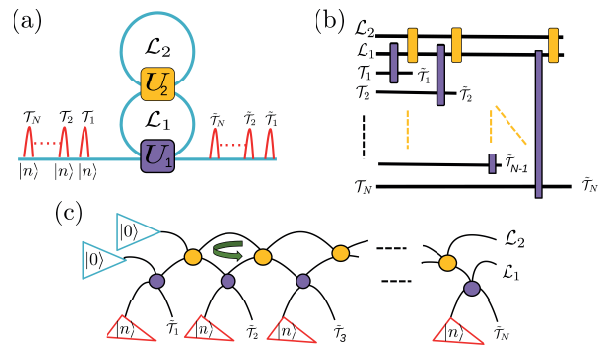


FIG. 10. (a) A tower of two ancillary fiber loops \mathcal{L}_1 and \mathcal{L}_2 is interacting with a train of input time-bin modes \mathcal{T}_i of photon numbers n_i and generating a train of output time-bin modes $\tilde{\mathcal{T}}_i$. (b) The circuit is composed of a ladder of identical coupler gates realizing the unitary interaction \hat{U}_1 (purple) between the input time-bin modes \mathcal{T}_i and \mathcal{L}_i at time-step i . Note that, different from Fig. 2, now the fiber loop system \mathcal{L} does not move one step down the ladder after every coupling interaction. Each interaction \hat{U}_1 is followed by a coupler interaction \hat{U}_2 (yellow) between the two fiber loop modes \mathcal{L}_1 and \mathcal{L}_2 . (c) The corresponding tensor network state is obtained by replacing the coupling gates \hat{U}_1 (purple) and \hat{U}_2 (yellow) at each time-step i by their corresponding graph vertices. The input states of the loop and time-bin modes are the blue and red triangles, respectively, which represent tensors of rank one. The green arrow highlights a closed loop in the tensor network state.

beam splitter \hat{U}_1 between the first loop \mathcal{L}_1 and the input time-bin mode \mathcal{T}_i at time-step i is followed by a beam splitter \hat{U}_2 between the two loop modes. It is straightforward to obtain the tensor network graph for the output state from the circuit diagram: we just need to identify the initial states and gates as the vertices in the tensor network state. We can see in Fig. 10 (c) that the double layer of ancillary loop modes generates closed loops in the tensor network representation. Clearly we could go beyond this and generate even more loops in the tensor network graph and thus even more complex tensor network states, simply by including more fiber loops in the ancillary system.

2. Concatenating fiber loops

An alternative approach for the generation of tensor network states with cycles is given by concatenating fiber loops. In Fig. 4 we can see that the horizontal edges of the tensor network graph correspond to the physical indices of the fiber loop mode \mathcal{L} at different time-steps i and the vertical edges correspond to the input and output time-bin modes \mathcal{T}_i and $\tilde{\mathcal{T}}_i$, respectively, where the latter are open, i.e. not contracted, indices as they correspond to the physical indices of the final state. When we concatenate two fiber loops, as depicted in Fig. 11 (a), the output time-bin modes of the first loop \mathcal{L}_1 become the

² A simple cycle is a path of vertices and edges in which each vertex can be reached from itself via a sequence of vertices starting and ending at the same vertex with no repetitions of vertices and edges allowed except for the starting and ending vertex.

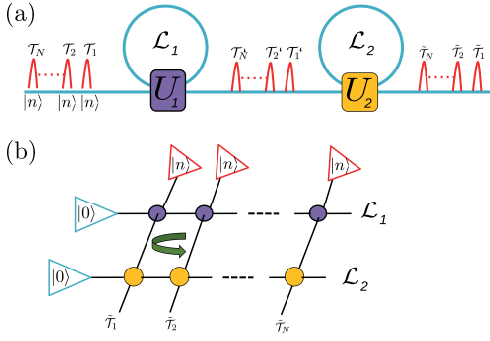


FIG. 11. (a) Scheme of two concatenated fiber loops \mathcal{L}_1 and \mathcal{L}_2 , where \mathcal{T}_i and $\tilde{\mathcal{T}}_i$ represent input and output time-bin modes, respectively, \mathcal{T}'_i represent the time-bin modes in the middle of the interferometer. \hat{U}_1 and \hat{U}_2 are beam splitters. (b) Tensor network representation of the output state for N time-bin modes after passing through the two fiber loops. The purple/yellow circles represent tensors with two input and two output indices where each index corresponds to either an input or output degree of freedom of the coupling interaction \hat{U}_1/\hat{U}_2 . The blue and red triangles represent tensors with one index and this index corresponds to the input state of the loop and time-bin modes, respectively.

input modes of the second fiber loop \mathcal{L}_2 . This creates a tensor network graph with an additional horizontal line, shown in Fig. 11 (b), that encodes the evolution of the internal degree of freedom of the second fiber loop \mathcal{L}_2 over time. Note that because the coupling interactions \hat{U}_1 and \hat{U}_2 are time-invariant, all the tensors in the first and second horizontal line are the same, respectively.

3. Multiple parallel time-bin chains

The tensor network formalism that we have just described for the tower and concatenation of fiber loops can be extended to more general interferometric schemes, composed of any number of fiber loops or time-bin modes in arbitrary architectures. Additionally, we could also have multiple input and output trains of time-bin pulses that interact with each other simultaneously through a complex network of fiber loops. As an example, Fig. 12 shows how tritters, i.e. three-mode interferometers, can be used to generate a very complex tensor network, namely a projected entangled pair state with cylindrical boundary conditions.

It is also not difficult to see that one can alternatively generate a tensor network with cylindrical boundary conditions using a tower of two loops, as in Fig. 10, by choosing the first loop \mathcal{L}_1 to be larger than the second loop \mathcal{L}_2 .

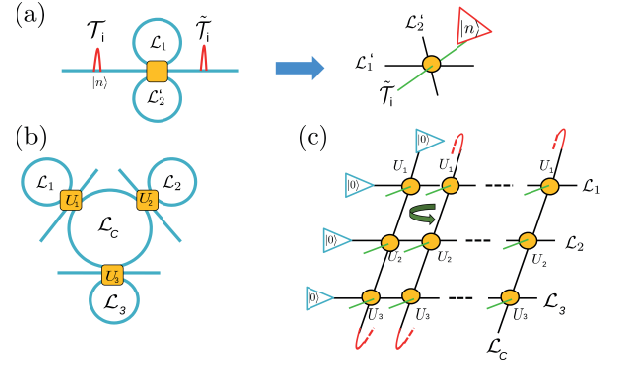


FIG. 12. (a) A tritter interaction is defined by a unitary with three inputs and three outputs. For a fixed time-step i and input time-bin \mathcal{T}_i , after contraction of the input state $|n\rangle$ (red triangle) with the tritter vertex, we obtain a tensor with five indices where four indices correspond to the two initial and final fiber loop modes and the remaining index corresponds to the output time-bin mode $\tilde{\mathcal{T}}_i$ (green edge). (b) Three tritters have a local fiber loop each, \mathcal{L}_1 , \mathcal{L}_2 , and \mathcal{L}_3 , and a commonly shared fiber loop \mathcal{L}_C . (c) This generates a projected entangled pair state with cylindrical boundary conditions. The cylindrical boundary conditions result from the fact that every final vertical edge of a given column of the graph, leaving a \hat{U}_3 vertex, becomes the uppermost vertical input edge, entering a \hat{U}_1 vertex of the following column.

B. Hard instances

The intuition that the computational complexity of a tensor network contraction increases with the number of simple cycles contained in the tensor network graph can be formulated mathematically via the concept of the treewidth of a graph. This is a computable quantity that quantifies how far a graph is from being acyclic [60].

1. Treewidth of a graph

A tree graph, or acyclic graph, is a graph where every path between two vertices is unique, see Fig. 13 (b) for an example. As shown in Ref. [60] a tree tensor network can be contracted efficiently, where the running time scales polynomially with the number of vertices and the bond dimension. Note that a tree tensor network graph is more general than a one-dimensional chain, and thus a matrix product state, as it may contain attached branches.

For a cyclic graph, such as the one in Fig. 13 (a), the notion of tree decomposition is an ensemble of operations that maps every vertex v of a tree graph G_{tree} into a subset $B(v)$ of vertices of the initial cyclic graph G , called bags. The mapping must satisfy the following three rules:

- Each vertex of G must appear in at least one bag.
- For each edge of G at least one bag must contain both of its end vertices.

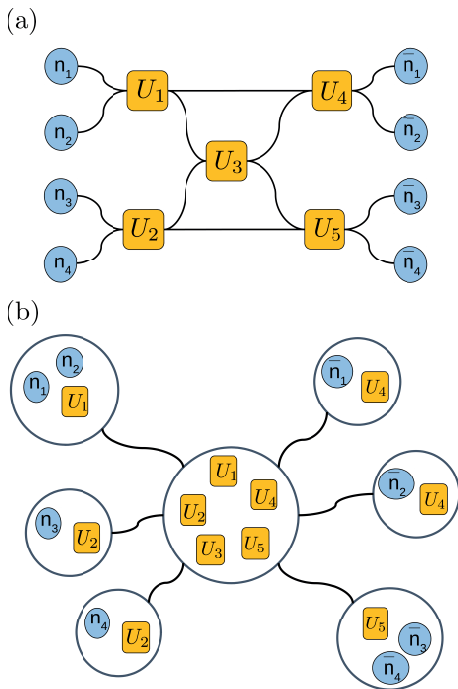


FIG. 13. (a) This tensor network G represents the evolution of four initial states with photon numbers n_1 to n_4 over a set of five couplers U_1 to U_5 and leads to measurement outcomes of photon numbers \bar{n}_1 to \bar{n}_4 . (b) A tree decomposition results from creating bags that contain tensors of G following the three rules explained in the main text just above Eq. (11). The width of this decomposition is four, as the largest bag – namely the the central one – contains five tensors.

- For a every vertex v of G the set of vertices of G_{tree} such that their corresponding bags contain v form a connected subtree.

The width of a given tree decomposition is defined as

$$\text{width}(G_{\text{tree}}) := \max_{v \in V(G_{\text{tree}})} |B(v)| - 1 \quad (11)$$

where $|B(v)|$ is the size of the bag corresponding to vertex v of G_{tree} , see Ref. [60] for details. For a specific tree decomposition, it is easy to calculate its width. But a given cyclic graph can have different decompositions of different widths. Therefore, we define the treewidth $\text{tw}(G)$ as the minimum width over all the possible tree decompositions of G , and this quantifies how far the graph is from a tree. The exact calculation of the treewidth of a general tensor network – which is equivalent to finding the optimal tensor contraction order – is an NP-complete problem [61, 62].

2. Sufficient condition for efficient simulation

If we want to adapt the main result of Ref. [60] to the harmonic oscillator setup of quantum optics, then we

need to take the possible bunching of photons into account. This can be achieved by defining the local dimension d of every tensor to be as large as the total number of photons M plus one, $d = M + 1$.

Theorem 2. Let G_A denote the tensor network graph for a photonic architecture A of N modes containing a maximum total number of M photons and T couplers. Then the output probability distribution of local measurements can be deterministically computed in poly($TM^{\mathcal{O}(\text{tw}(G_A))}$) time.

As opposed to the tensor contraction of finite-dimensional systems (qudits, spins) where a treewidth scaling logarithmically with the size of the system leads to a poly($\text{tw}(G)$) time algorithm, here we obtain a quasi-polynomial time algorithm for logarithmically scaling treewidth. We could restore the polynomial scaling occurring in finite-dimensional systems if we could truncate the physical dimension d to a constant value, e.g. to a few times the average photon number on each mode, an efficiently computable quantity. Unfortunately, it is non-trivial to prove that such an approach leads to an algorithm that can approximate the tensor network contraction with error ϵ and has a running time that scales polynomially both in $1/\epsilon$ and the size of the system, M and N . This proof is a task that we leave for future work.

Although the calculation of the treewidth is NP-complete, finding an upper bound that is sub-logarithmic is sufficient to prove that a tensor network has an efficient contraction, and that is a simpler task than finding the optimal contraction. In order to prove the hardness of a tensor contraction one needs to show that the treewidth has a super-logarithmic lower bound, which for some classes of graphs is easy to do. E.g. a lattice graph G with $|V(G)|$ vertices has a treewidth scaling as $\sqrt{|V(G)|}$.

3. A route to resilient quantum advantage architectures

One of the most pursued routes to quantum advantage is based on searching for non-universal and easy to implement quantum architectures that generate sampling distributions that are hard to reproduce by a classical computer. Boson sampling is the quantum optical route to quantum advantage, which has attracted a lot of interest from both theoreticians and experimentalists. As in other quantum advantage proposals, the effects of experimental imperfections, such as losses or distinguishability of photons or noise, will be crucial in a real experimental demonstration. Therefore, searching for novel photonic architectures that are more resilient to those imperfections is crucial if we want to experimentally demonstrate quantum advantage.

The main path to prove hardness of sampling in a given quantum architecture is to prove that at least one probability outcome is #P-hard to compute (for exact sampling) or most instances are #P-hard to compute (for approximate sampling). Because the hardest instances of tensor networks are #P-hard to contract [40], it is

tempting to leverage all knowledge accumulated about tensor networks in order to search for good candidates of a quantum advantage architecture. In this direction the previous theorem is a very useful tool that allows us to discard some photonic architectures that are classically simulatable. At the same time this theorem provides hints of where to look for good architectures that are computationally hard for sampling but less demanding in the number of resources and more resilient to imperfections than current proposals. E.g. we might be able to trade off depth of the circuit of current boson sampling proposals, which usually results in added losses in the real experiment, by moving from a planar circuit architecture to a three-dimensional structure that generates tensor networks of similar treewidths than the corresponding planar circuit but in a more compact volume and therefore reduces the losses and the noise. We leave further exploration of this for future work.

VI. CONCLUSIONS AND OUTLOOK

In this article we formulated time-bin linear quantum optics in the framework of tensor network states. This allowed us to make a first step towards using tensor network states for the simulation and design of large quantum optical experiments.

First we focussed on a single fiber loop and demonstrated that it has an efficient matrix product state representation. We extensively investigated quantities natural in many-body physics, such as the entanglement entropy and the correlations in the system. We proved an area law for the single fiber loop architecture and showed numerically that our area law upper bound is tight and experimentally achievable. We also observed an exponential decay of correlations and of Schmidt coefficients, which together with the area law, are consistent with a matrix product state representation of finite bond dimension that is classically efficiently simulatable.

We discussed the connection between interferometric loops and cycles in the tensor network representation, known to be the source of increasing computational complexity within the tensor network framework. Then we showed how to build more complex setups composed of several fiber loops and tritters, and we demonstrated that these experimental setups can generate tensor networks, such as projected entangled pair states, whose contraction is known to be hard. Finally, we have shown that

tensor network states are a useful tool to guide the design of future boson sampling quantum advantage experiments.

Despite the fact that the numerical simulation of the single fiber loop setup is computationally feasible, the unbounded nature of the optical modes adds an additional degree of complexity to the numerical simulation. In order to obtain accurate numerical results we needed to set the physical dimension of the system to be one order of magnitude larger than the average number of photons per mode. Interestingly, we observed that for our quantum optical simulations the bond dimension and the physical dimension could be treated in the same way.

An interesting next step is the development of novel numerical tensor network techniques tailored to the unbounded nature of the quantum optical scenario. A possible approach, inspired by the similarities between the bond and the physical dimension, would be the development of approximation algorithms that truncate the physical dimension along the tensor network. Algorithms already exist that can efficiently compute approximations of projected entangled pair state contractions and provide estimates of the approximation errors, see e.g. Refs. [41, 42]. It is tempting to apply these methods to classically simulate the boson sampling experiments proposed in Sec. V. This would allow us to refine the boundary between boson sampling experiments that can and cannot be currently classically simulated, using state-of-the-art tensor network methods.

During the completion of this article we learned about Ref. [63] that also discusses the use of tensor networks to simulate quantum optical experiments.

VII. ACKNOWLEDGEMENTS

M.L. acknowledges funding from the Networked Quantum Information Technologies Hub (NQIT) of the UK National Quantum Technology Programme as well as from the EPSRC grant ‘‘Tensor Network Theory for strongly correlated quantum systems’’ (EP/K038311/1). J.J.R. acknowledges NWO Rubicon. MSK acknowledges the Royal Society and the Samsung GRO grant. I.W. acknowledges ERC Advance Grant MOQUACINO. R.G.-P. is Research Associate of the F.R.S.-FNRS. R.G.-P. and I. W. acknowledge funding from the Fondation Wiener-Anspach. A.A.V. thanks German Sierra and Juan Jose Garcıa-Ripoll for helpful discussions. We are also grateful to Joelle Boutari for helpful discussions.

[1] A. W. Harrow and A. Montanaro, *Nature* **549**, 203 (2017).
 [2] A. A. Aaronson and A. Arkhipov, *Proceedings of STOC11 43rd Annual ACM Symposium on Theory of Computing*, 333 (2011).
 [3] A. Schreiber *et al.*, *Phys. Rev. Lett.* **104**, 050502 (2010).

[4] S. K. Goyal *et al.*, *Phys. Rev. Lett.* **110**, 263602 (2013).
 [5] F. Cardano *et al.*, *Sci. Adv.* **1**, e1500087 (2015).
 [6] M. Pant and D. Englund, *Phys. Rev. A* **93**, 043803 (2016).
 [7] K. R. Motes *et al.*, *Phys. Rev. Lett.* **113**, 120501 (2014).
 [8] Y. He *et al.*, *Phys. Rev. Lett.* **118**, 190501 (2017).

- [9] A. Schreiber *et al.*, *Science* **336**, 55 (2012).
- [10] J. Boutari *et al.*, *J. Opt.* **18**, 094007 (2016).
- [11] S. Takeda and A. Furusawa, *Phys. Rev. Lett* **119**, 120504 (2017).
- [12] C. Want *et al.*, *Opt. Expr.* **22**, 30924 (2014).
- [13] E. L. Wooten *et al.*, *IEEE J. Sel. Topics Quantum Electron.* **6**, 69 (2000).
- [14] I. Krasnokutska, arXiv:1708.06787 (2017).
- [15] F. Verstraete, V. Murg, and J. I. Cirac, *Adv. Phys.* **57**, 143 (2008).
- [16] J. I. Cirac and F. Verstraete, *J. Phys. A: Math. Theor.* **42**, 504004 (2009).
- [17] J. Eisert, *Modeling and Simulation* **3**, 520 (2013).
- [18] R. Orús, *Ann. Phys.* **349**, 117158 (2014).
- [19] S. Iblisdir, R. Orús, and J. I. Latorre, *Phys. Rev. B* **75**, 104305 (2007).
- [20] M. Ohliger, K. Kieling, and J. Eisert, *Phys. Rev. A* **82**, 042336 (2010).
- [21] M. Ohliger and J. Eisert, *Phys. Rev. A* **85**, 062318 (2012).
- [22] K. Temme and P. Wocjan, arXiv:1208.6589 (2012).
- [23] M. Jarzyna and R. Demkowicz-Dobrzański, *Phys. Rev. Lett.* **110**, 240405 (2013).
- [24] R. A. Campos, B. E. A. Saleh, and M. C. Teich, *Phys. Rev. A* **40**, 1371 (1989).
- [25] M. Kim, W. Son, V. Buzek, and P. L. Knight, *Phys. Rev. A* **65**, 032323 (2002).
- [26] S. R. White, *Phys. Rev. Lett.* **69**, 2863 (1992).
- [27] U. Schollwöck, *Rev. Mod. Phys.* **77**, 259 (2005).
- [28] S. Östlund and S. Rommer, *Phys. Rev. Lett.* **75**, 3537 (1995).
- [29] F. Verstraete, D. Porras, and J. I. Cirac, *Phys. Rev. Lett.* **93**, 227205 (2004).
- [30] U. Schollwöck, *Ann. Phys.* **326**, 96 (2011).
- [31] M. Fannes, N. Nachtergaele, and R. F. Werner, *Commun. Math. Phys.* **114**, 443 (1992).
- [32] G. Vidal, *Phys. Rev. Lett.* **91**, 147902 (2003).
- [33] D. Pérez-García, F. Verstraete, M. Wolf, and J. I. Cirac, *Quantum Inf. Comp.* **7**, 401 (2007).
- [34] M. A Nielsen and I. L. Chuang, *Quantum Computation and Quantum Information*, Cambridge University Press (2010).
- [35] Ch. H. Bennett, H J. Bernstein, S. Popescu, and B. Schumacher, *Phys. Rev. A* **53**, 2046 (1996).
- [36] R. Horodecki, P. Horodecki, M. Horodecki, and K. Horodecki, *Rev. Mod. Phys.* **81**, 865 (2009).
- [37] N. Schuch, M. M. Wolf, F. Verstraete, and J. I. Cirac, *Phys. Rev. Lett.* **100**, 030504 (2008).
- [38] F. Verstraete and J. I. Cirac, arXiv:cond-mat/0407066 (2004).
- [39] V. Murg, F. Verstraete, and J. I. Cirac, *Phys. Rev. A* **75**, 033605 (2007).
- [40] N. Schuch, M. M. Wolf, F. Verstraete, and J. I. Cirac, *Phys. Rev. Lett.* **98**, 140506 (2007).
- [41] M. Lubasch, J. I. Cirac, and M.-C. Bañuls, *New J. Phys.* **16**, 033014 (2014).
- [42] M. Lubasch, J. I. Cirac, and M.-C. Bañuls, *Phys. Rev. B* **90**, 064425 (2014).
- [43] A. Perelomov, *Generalized coherent states and some of their applications*, Springer-Verlag (1986).
- [44] S. D. Bartlett and B. C. Sanders, *Phys. Rev. Lett.* **89**, 207903 (2002).
- [45] A. Mari and J. Eisert, *Phys. Rev. Lett.* **109**, 203503 (2012).
- [46] V. Veitch, N. Wieve, C. Ferrie, and J. Emerson, *New J. Phys.* **15**, 013307 (2013).
- [47] S. Rahimi-Keshari, T. C. Ralph, and C. M. Caves, *Phys. Rev. X* **6**, 021039 (2016).
- [48] C. Schön, E. Solano, F. Verstraete, J. I. Cirac, and M. M. Wolf, *Phys. Rev. Lett.* **95**, 110503 (2005).
- [49] C. Schön, K. Hammerer, M. M. Wolf, J. I. Cirac, and E. Solano, *Phys. Rev. A* **75**, 032311 (2007).
- [50] M. B. Hastings, *J. Stat. Mech.* **2007**, P08024 (2007).
- [51] J. Eisert, M. Cramer, and M. B. Plenio, *Rev. Mod. Phys.* **82**, 277 (2010).
- [52] F. Verstraete and J. I. Cirac, *Phys. Rev. B* **73**, 094423 (2006).
- [53] Z. Landau, U. Vazirani, and T. Vidick, *Nat. Phys.* **11**, 566 (2015).
- [54] J. J. Sakurai and J. Napolitano, *Modern Quantum Mechanics*, Cambridge University Press (2017).
- [55] M. M. Wolf, G. Giedke, and J. I. Cirac, *Phys. Rev. Lett.* **96**, 080502 (2006).
- [56] S. Al-Assam, S. R. Clark, and D. Jaksch, *J. Stat. Mech.* (2017) 093102.
- [57] The Tensor Network Theory Library is an open-source software project and available at <http://www.tensornetworktheory.org>.
- [58] M. Walschaers *et al.*, *New J. Phys.* **18**, 032001 (2016).
- [59] R. Diestel, *Graph Theory*, Springer-Verlag (2005).
- [60] I. L. Markov and Y. Shi, *SIAM J. Comput.* **38**, 963981 (2008).
- [61] H. L. Bodlaender, *Classes of graph with bounded treewidth*, Department of computer science, Utrecht University (1986).
- [62] H. L. Bodlaender, *Discovering treewidth*, Institute of information and computing sciences, Utrecht University (2005).
- [63] I. Dhand, M. Engelkemeier, L. Sansoni, S. Barkhofen, C. Silberhorn, and M. B. Plenio, arXiv:1710.06103 (2017).